Draft version October 22, 2025
Typeset using LaTeX **twocolumn** style in AASTeX7

The Growth of the Central Black Holes in Quasi-stars

Jake B. Hassan [1], Rosalba Perna [1], Matteo Cantiello [2,3], Philip J. Armitage [1,2], Mitchell C. Begelman [4,5] and Taeho Ryu [4,5,6]

[1] *Department of Physics and Astronomy, Stony Brook University, Stony Brook, NY 11794-3800, USA*
[2] *Center for Computational Astrophysics, Flatiron Institute, 162 5th Avenue, New York, NY 10010, USA*
[3] *Department of Astrophysical Sciences, Princeton University, Princeton, NJ 08544, USA*
[4] *JILA, University of Colorado and National Institute of Standards and Technology, 440 UCB, Boulder, CO 80309-0440, USA*
[5] *Department of Astrophysical and Planetary Sciences, University of Colorado, 391 UCB, Boulder, CO 80309-0391, USA*
[6] *Max-Planck-Institut für Astrophysik, Karl-Schwarzschild-Straße 1, 85748 Garching bei München, Germany*

(Received; Revised; Accepted)

ABSTRACT

Observations by JWST have confirmed the presence of supermassive black holes (BHs) at redshifts $z \gtrsim 10$, lending support to scenarios in which BHs experience rapid growth through intense gas accretion. Here we investigate the growth of a BH embedded at the center of a quasi-star, a theoretically predicted object formed via direct collapse. In a quasi-star, the central BH accretes at a highly super-Eddington rate, while the excess energy is transported outward by convection and radiated at approximately the Eddington luminosity of the entire star. We employ the open-source stellar evolution code `MESA` to construct quasi-star models and follow the time-dependent growth of the central BH under different prescriptions for the accretion rate at the inner boundary R_i, and further considering the effect of winds. For the case $R_i = NR_{\rm B}$, where N is a constant and $R_{\rm B}$ is the Bondi radius corresponding to the mass of the BH and the gas infalling onto it, our models terminate when the BH mass reaches a critical value $M_{\rm crit}(N) = c_{s,i}^3/(12\sqrt{N^3G^3\pi\rho_i})$ (where $c_{s,i}$ and ρ_i are the sound speed and density at R_i, respectively), a limit we also derive analytically. Models that feature an inner convective region matched to an outer adiabatic envelope exhibit BH growth up to approximately $M_{\rm BH}/M_\star \simeq 0.33$, largely independent of the stellar mass $M_\star$ itself. This ratio is approximately preserved even in the presence of mass loss, as several properties of the model are independent of the quasi-star's total mass.

Keywords: Early Universe — Accretion — Black hole physics — Quasars

1. INTRODUCTION

One of the central challenges in modern astrophysics is explaining the rapid emergence of supermassive black holes (SMBHs) within the first billion years of the universe. Observations of quasars at redshifts $z \gtrsim 6$ imply that black holes with masses $\gtrsim 10^9\,M_\odot$ were already in place less than a Gyr after the Big Bang (X. Fan et al. 2006; E. Bañados et al. 2018). The conventional growth of black holes (BHs) from stellar-mass seeds through Eddington-limited accretion struggles to meet these stringent timescales, prompting the exploration of more rapid or exotic formation pathways. Among these, quasi-stars —massive, extended, radiation-pressure supported envelopes surrounding growing BH seeds—have long been proposed as a viable mechanism for early black hole growth (M. C. Begelman et al. 2006, 2008; M. Volonteri & M. C. Begelman 2010; W. H. Ball et al. 2011).

Quasi-stars form when a dense gas cloud undergoes direct collapse of its core region, leading to the formation of a central BH embedded within a massive envelope. The envelope feeds the BH through a convective, radiation-dominated accretion flow, while carrying away the liberated energy and ultimately radiating most of it away at a star-like photosphere. Because the quasi-star envelope absorbs and reprocesses the accretion luminosity, the BH can grow at rates well above the Eddington limit for isolated accretion, reaching intermediate

Corresponding author: Jake B. Hassan
jakebhassan@gmail.com

masses ($\sim 10^3$–$10^4\,M_\odot$) or higher on short timescales of less than a few Myr (M. C. Begelman et al. 2008). Models of quasi-stars must make choices for several physically uncertain processes, including the efficiency of energy transport in the envelope, the appropriate inner boundary conditions, the treatment of density inversions, and the strength of winds (C. Dotan et al. 2011; D. Fiacconi & E. M. Rossi 2017). These processes determine the quasi-stars' hydrostatic stability, and, given some assumed ongoing accretion rate, the mass of the BH that emerges at the end of the quasi-star phase. Notably, W. H. Ball et al. (2011, 2012), constructing quasi-star models with the Cambridge `STARS` evolution code and a free-fall model for the inner region (M. C. Begelman et al. 2008) found that the central BH cannot grow beyond a few percent of the total quasi-star mass $M_\star$. More recently, however, E. R. Coughlin & M. C. Begelman (2024) revisited the internal structure of quasi-stars using a more physically realistic treatment of the inner boundary condition at the BH's radius of influence. Their results demonstrated that a substantially larger fraction of the envelope mass can be accreted, leading to a BH mass $\sim 0.62 M_\star$, and significantly enhancing the plausibility of quasi-stars as progenitors of the SMBHs powering high-redshift quasars.

At the same time, recent observational discoveries have revived interest in the quasi-star hypothesis. Deep imaging from the *James Webb Space Telescope* (JWST) has revealed a population of faint, red, compact sources—dubbed "Little Red Dots" (LRDs)— at redshifts $z \sim 6$–10. Their spectral energy distribution is characterized by a "V"-shaped spectrum in the rest-frame continuum between the UV and the optical, with a turnover near the Balmer break (e.g. I. Labbé et al. 2023; L. J. Furtak et al. 2023; G. Barro et al. 2024; J. E. Greene et al. 2024; V. Kokorev et al. 2024; J. Matthee et al. 2024; D. J. Setton et al. 2024; H. B. Akins et al. 2025; D. D. Kocevski et al. 2025; A. J. Taylor et al. 2025). Most of them display broad, typically exponentially-shaped lines and lack X-ray emission, possibly an indication of high column densities.

The physical origin of LRDs remains uncertain, with possibilities ranging from heavily dust-enshrouded star-forming galaxies to black holes accreting via geometrically thick super-Eddington flows in an early growth phase (H. Liu et al. 2025). Quasi-stars naturally predict red, compact, low-temperature emission due to their extended envelopes and reprocessed luminosity, and have therefore emerged as compelling candidates to explain at least a subset of the LRD population (M. C. Begelman & J. Dexter 2025).

In this work, we investigate the connection between quasi-stars and the rapid growth of massive BH seeds by constructing detailed models of quasi-star structure and evolution, motivated by the recent theoretical and observational developments discussed above. We employ the stellar evolution code `MESA` (B. Paxton et al. 2011, 2013, 2015, 2018, 2019) to model the time-dependent evolution of quasi-stars and the corresponding growth of their central BHs. Our analysis focuses on assessing the impact of the adopted inner boundary condition, as well as of mass loss, on the final BH mass, with the goal of determining whether the central BH can ultimately grow to a significant fraction of the total quasi-star mass.

Our paper is organized as follows. In Section 2.1, we describe the numerical methods employed in this work. In Section 2.2, we present our implementation of the framework developed by W. H. Ball et al. (2011, 2012), and derive an analytical expression for the maximum BH mass attainable within their model, demonstrating excellent agreement with the numerical evolution obtained using `MESA`. In Section 2.3, we detail our implementation of the inner boundary conditions following E. R. Coughlin & M. C. Begelman (2024), and inclusive of the more recent updates by M. C. Begelman & J. Dexter (2025), while Section 2.4 describes our treatment of mass loss. The results of the numerical evolution within this framework are presented in Section 3, studying first models without winds (Section 3.1) and then considering the effect of winds (Section 3.2). Last, our conclusions and summary are provided in Section 4.

2. STRUCTURE AND EVOLUTION OF QUASISTARS

2.1. *Numerical methods*

We use version r24.08.1 of the open-source stellar evolution code Modules for Experiments in Stellar Astrophysics (`MESA`; B. Paxton et al. 2011, 2013, 2015, 2018, 2019) to construct evolutionary models of quasi-stars. `MESA` is a one-dimensional numerical tool designed to model stellar structure and evolution across a broad range of stellar masses, chemical compositions, and evolutionary stages. It solves the coupled stellar structure equations using an implicit scheme with adaptive timesteps and incorporates multiple tabulated equations of state that span extensive ranges of temperature, density, and composition.

Our extension of the `MESA` code is largely built upon the work of E. P. Bellinger et al. (2023), who focused on Sun-like models containing primordial BHs. We first initialize a supermassive star with $X = 0.7$, $Y = 0.3$, $Z = 0$. We allow the star to relax to thermal equi-

librium, at which point we inject a BH of initial mass $M_{\rm BH,init} = 0.01\ {\rm M}_\star$ into the center.

MESA only models the portion of the star in hydrostatic equilibrium (HSE); in the case of conventional stars, the inner boundary conditions for this region, located above the inner radius R_i, would be $R_i = 0, M(R_i) = 0, L(R_i) = 0$. In the case of a quasi-star, the region in HSE forms an envelope around a non-HSE interior gravitationally dominated by the BH. As the quasi-star evolves, we calculate the BH's mass at each time step, use this to determine new inner boundary conditions for the envelope, and then have MESA model the envelope from those boundary conditions.

Nuclear fusion is neglected within the region dominated by the BH. In our models, hydrogen burning does occur during the relaxation phase, as well as near the base of the envelope shortly after the BH is introduced. However, temperatures in the envelope quickly drop and become too low for fusion.

We found that excessively large time steps lead to oscillations in the envelope luminosity, density, and pressure. To mitigate this, we implemented an adaptive time-step control scheme that reduces the step size whenever the luminosity varies too rapidly. The time step is then gradually increased again until renewed fluctuations trigger another reduction. This approach effectively suppresses the variability while preserving a computationally efficient evolutionary timescale for the model.

2.2. *Inner Boundary Condition: Comparison with previous work and with new analytical results*

As a first study case, we implement the models described in W. H. Ball et al. (2011, 2012) (henceforth referred to as the "Ball model"). During our work on this project, C. B. Campbell et al. (2025) released a similar implementation of W. H. Ball et al. (2011) in MESA. Like our implementation, theirs was based on E. P. Bellinger et al. (2023); they additionally incorporated the Tolman-Oppenheimer-Volkoff (TOV) correction, as well as a mechanism to spatially smooth several physical quantities in order to reduce fluctuations. In light of this, we added the TOV correction to our version. We do not incorporate their smoothing mechanism, but it served as inspiration for our own solution of slowing down time steps when the fluctuations begin.

Assuming the region dominated by the BH is a sphere of some radius R_i, the mass at the envelope's inner boundary is

$$M_i = M_{\rm BH} + M_{\rm cav}\,, \tag{1}$$

where $M_{\rm cav}$ corresponds to the gaseous material under the gravitational influence of the BH. Assuming $\rho(r) \propto r^{-3/2}$, this is given by $M_{\rm cav} = \frac{8\pi}{3}\rho_i R_i^3$, where ρ_i is the density at R_i.

W. H. Ball et al. (2011) took R_i to be a multiple of the Bondi radius (H. Bondi 1952) of the BH,

$$R_i = N\frac{2GM_{\rm BH}}{c_{s,i}^2}, \tag{2}$$

where N is a tunable parameter (assumed to be $N = 1$ in their paper, so that R_i effectively becomes the Bondi radius of the BH). Here, $c_{s,i}$ is the sound speed at R_i, which is related to the density and total pressure by $c_{s,i} = \sqrt{4p_i/3\rho_i}$.

W. H. Ball et al. (2011) noted that energy produced by the BH is transmitted out of the interior via convection. Because the maximum energy flux achievable by convection is $F = pc_s$, the luminosity L would be capped by the maximum convective luminosity in the region, $L_{\rm conv} = 4\pi R_i^2 p_i c_{s,i}$ (M. C. Begelman et al. 2008). By introducing a convective efficiency η, the accretion luminosity can be expressed as

$$L = 4\eta\pi R_i^2 p_i c_{s,i}\,. \tag{3}$$

Moreover, the luminosity of the quasi-star is assumed to be produced entirely by the conversion of mass accreted by the BH into radiation. Denoting ϵ as the radiative efficiency and defining $\epsilon' = \epsilon/(1-\epsilon)$, we have $\dot{M}_{\rm BH} = (1-\epsilon)\dot{M}_{\rm in}$ and

$$L = \epsilon\dot{M}_{\rm in}c^2 = \epsilon'\dot{M}_{\rm BH}c^2. \tag{4}$$

In the above equation, $\dot{M}_{\rm in}$ represents the mass inflow rate across the base of the envelope of the quasi-star towards the BH. Note that the system as a whole loses some mass to radiation via this mechanism, at a rate of $L/c^2 = \epsilon\dot{M}_{\rm in}$. Here, for simplicity of notation, we always indicate with $M_\star$ the total instantaneous mass of the star. As with W. H. Ball et al. (2011), we assume $\epsilon = \eta = 0.1$. Using Equation 3, we can compute L once R_i has been calculated (with the pressure p_i and sound speed $c_{s,i}$ at the boundary being computed by MESA). We can then obtain $\dot{M}_{\rm BH}$ from Equation 4, which we use to linearly approximate the BH's mass at the next step of the model. With this, we can likewise estimate the remaining boundary conditions at the next time step.

Figure 1 shows the results for our MESA implementation of the model from W. H. Ball et al. (2011), for different values of N in Equation 2. Our results are consistent with those of W. H. Ball et al. (2011) and C. B. Campbell et al. (2025).

W. H. Ball et al. (2012) corrected the inner boundary condition of this model to account for the gravitational influence of the infalling gas, by replacing $M_{\rm BH}$ with

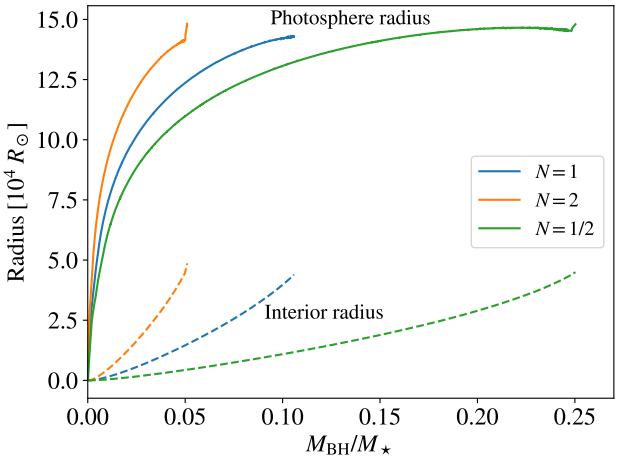

Figure 1. The radii of the photosphere (solid) and interior region R_i (dashed) for a $M_\star = 10^5 M_\odot$ quasi-star as a function of the BH mass normalized by the instantaneous stellar mass, with our `MESA` implementation of the W. H. Ball et al. (2011) model for different values of the parameter N (cf. Eq. 2). All models are initialized with the same properties and an initial BH mass of $M_{\rm BH} = 100 M_\odot$.

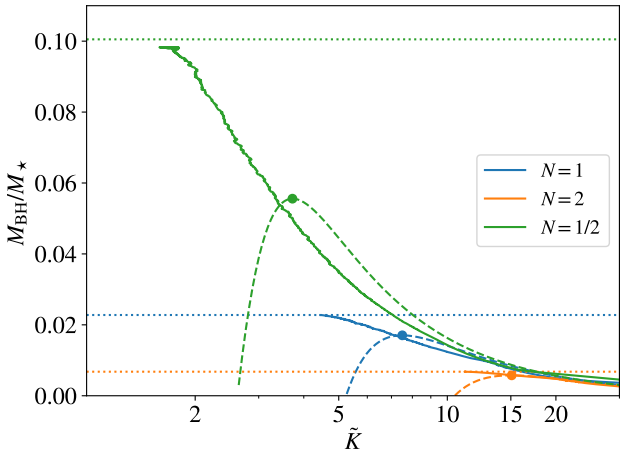

Figure 2. Solid lines: Ratio between BH and star mass as a function of the dimensionless entropy, and for different values of the parameter N in our `MESA` implementation of the Ball model. The numerical curves are plotted until the end of the `MESA` simulations. Dotted horizontal lines indicate our analytically derived maximum mass in the Ball model, $M_{\rm crit}(N)$ (Eq. 5). Also shown with dashed curves are the analytical solutions of E. R. Coughlin & M. C. Begelman 2024, with the maximum BH masses predicted by their solutions marked with filled circles.

$M_i = M_{\rm BH} + \frac{8\pi}{3}\rho_i R_i^3$ in Equation 2. This yields a cubic equation for R_i, which has no physically valid solutions for BH masses above

$$M_{\rm crit}(N) = \frac{c_{s,i}^3}{12\sqrt{N^3 G^3 \pi \rho_i}}, \tag{5}$$

and has a unique valid solution when $M_{\rm BH} \leq M_{\rm crit}$:

$$R_i = \frac{6NGM_{\rm crit}}{c_{s,i}^2} \cos\left(\frac{1}{3}\arccos\left(\frac{M_{\rm BH}}{M_{\rm crit}}\right) + \frac{\pi}{3}\right). \tag{6}$$

A full derivation for this is given in Appendix A.

E. R. Coughlin & M. C. Begelman (2024) analytically estimated the maximum BH mass with this correction. They modeled the envelope with a 4/3 polytrope $p = K\rho^{4/3}$, and assumed this to be valid up to the photosphere of the quasi-star. They then computed the dimensionless entropy, defined by

$$\tilde{K} = \frac{4KM_i^{-2/3}}{G(4\pi)^{1/3}}, \tag{7}$$

and considered the maximum mass the BH could reach as $\tilde{K}$ gradually decreases. They found the maximum mass for the $N = 1$ case to be on the order of $M_{\rm BH}/M_\star \sim 0.01$, approximately an order of magnitude smaller than that of the Ball 2011 model.

In Figure 2 we compare our `MESA` implementation of the Ball 2012 model (solid lines) with the analytical predictions of E. R. Coughlin & M. C. Begelman (2024) (dashed lines), as well as with our analytically derived maximum BH mass $M_{\rm crit}(N)$ (cf. Eq. 5, marked with dotted lines corresponding to the various N). Our models were found to terminate well before reaching $R_i \approx R_\star$, with a maximum BH mass remarkably close to our analytical value $M_{\rm crit}(N)$. The final BH masses corroborate the analytical trend found by E. R. Coughlin & M. C. Begelman (2024) that the BHs reach higher limiting masses for lower values of N. However, for lower values of N, we reach higher BH masses than predicted by their analytical approximation. While the exact reason for this is unclear, it should be noted the analytical predictions are based on the assumptions that the convective envelope follows a $\gamma_o = 4/3$ polytrope, and that the atmosphere is thin (i.e. convective energy transfer remains efficient close to the surface of the quasi-star). We would expect any deviations from these idealizations to result in a slightly different maximum BH mass.

2.3. *Models with updated inner boundary condition*

Next, we implemented the model described in E. R. Coughlin & M. C. Begelman (2024) (which we refer to as the "Coughlin model"). As in the Ball model, the quasi-star is divided into an interior region dominated by a BH and an outer envelope that can be modeled by `MESA`. The luminosity is still assumed to be spatially constant and produced entirely from accretion. Physically, the difference is that the Ball model treats the interior region as a sphere of infalling gas, extending up to the

Bondi radius. In contrast, the Coughlin model treats the entire interior as carrying energy at the maximum rate achievable by convection, which is expected to be more accurate for high BH masses ($M_{\rm BH}/M_\star \gtrsim 0.1$).

In terms of implementation, the Ball model requires a means to compute R_i for a given BH mass (namely, the Bondi radius formula). From there, the luminosity condition is obtained by assuming $L = 4\eta\pi R_i^2 p_i c_{s,i}$ at the boundary (Equation 3). On the other hand, the Coughlin model requires a means to compute L for a given BH mass (as we discuss later, this is done by assuming L equals the Eddington luminosity of the quasi-star). We can then derive R_i by assuming $L = 4\eta\pi r^2 p c_s$ *everywhere* in the interior region, rather than only at the boundary.

This relation between the radius, density and (spatially constant) luminosity practically serves as an equation of state for the interior region of mass M_i. Defining the scaled radius and mass coordinates $\xi = r/R_i$ and $m_i = M(r)/M_i$, this leads to the Lane-Emden equation for the interior:

$$K_i \frac{d}{d\xi}\left[\xi^{-2}\left(\frac{dm_i}{d\xi}\right)^{1/3}\right] = -\frac{m_i}{\xi^4}\frac{dm_i}{d\xi} \tag{8}$$

where K_i is a constant satisfying

$$R_i = M_i (G K_i)^{3/5}\left(\frac{\eta\sqrt{\gamma_i}}{L}\right)^{2/5}. \tag{9}$$

Here, γ_i is the first adiabatic index in the interior. E. R. Coughlin & M. C. Begelman (2024) demonstrated that K_i is an invertible function of the ratio $M_{\rm BH}/M_i$.

To proceed further, assume that the convective portion of the envelope (adjacent to the interior region) can be described by a polytrope and has an adiabatic index of γ_o. Assume further that the mass, pressure and temperature are continuous when crossing R_i. From this, E. R. Coughlin & M. C. Begelman (2024) derived the Lane-Emden equation for this region:

$$\tilde{K}_o \frac{d}{d\xi}\left[\left(\xi^{-2}\frac{dm_o}{d\xi}\right)^{1/3}\right] = -\frac{m_o}{\xi^2} \tag{10}$$

where $m_o = M(r \geq R_i)/M_i$ and

$$\tilde{K}_o = \frac{\gamma_o}{\gamma_o - 1}\frac{K_i}{m_i'(1)^{\gamma_o - \frac{1}{3}}}. \tag{11}$$

E. R. Coughlin & M. C. Begelman (2024) demonstrates that the solutions to Equations 8 and 10 are uniquely determined by the value of K_i. The premise (skipping over the specifics in E. R. Coughlin & M. C. Begelman 2024) is that we can numerically solve both of these Lane-Emden equations at some $\xi = \xi_1$ in the interior and $\xi = \xi_2$ in the envelope. This gives $m_i(\xi_1)$ or $m_o(\xi_2)$, and K_i can be computed from either of them.

Of course, computing K_i this way would require knowledge of the values of either $m_i(\xi_1)$ or $m_o(\xi_2)$, which is not possible without knowing M_i a priori. However, suppose there exists a pair of (ξ_1, ξ_2) for which we know the masses $M(\xi_1)$ and $M(\xi_2)$. K_i is a function of $m_i(\xi_1) = M(\xi_1)/M_i$ and also a function of $m_i(\xi_2) = M(\xi_2)/M_i$, so it is a function of the ratio $m_i(\xi_1)/m(\xi_2) = M(\xi_1)/M(\xi_2)$, which would be calculable. Thus, we should choose a pair (ξ_1, ξ_2) for which we know the masses.

In the interior, the obvious choice is $\xi_1 = 0$, since $M(\xi = 0) = M_{\rm BH}$ is known a priori. In the exterior, all points in the polytropic envelope satisfy

$$\frac{1}{\xi^{3\gamma_o - 3}}\left(\frac{m_o'(\xi)}{m_o'(1)}\right)^{\frac{3\gamma_o - 1}{2}} = \frac{L_{\rm conv,max}(r)}{L}\sqrt{\frac{\gamma_i}{\gamma_o}}, \tag{12}$$

where $L_{\rm conv,max}(r) \equiv 4\pi\eta r^2 p c_s$ is the maximum convective luminosity achievable at radius r. From here, we assume $\gamma_i = \gamma_o = 4/3$, which reduces the above equation to

$$\frac{1}{\xi}\left(\frac{m_o'(\xi)}{m_o'(1)}\right)^{3/2} = \frac{L_{\rm conv,max}(r)}{L}. \tag{13}$$

If we now choose ξ_2 to be the point where $L = L_{\rm conv,max}$, we have

$$\frac{1}{\xi}\left(\frac{m_o'(\xi)}{m_o'(1)}\right)^{3/2} = 1. \tag{14}$$

E. R. Coughlin & M. C. Begelman (2024) took the condition $L = L_{\rm conv,max}$ to define the starting point of the quasi-star's radiative layer, where energy is primarily transported by radiation and the structure can no longer be described by the same polytropic model. They additionally assumed that the radiative layer was thin, such that the mass at this point is approximately $M_\star$. With these approximations, K_i could be computed using $M_{\rm BH}$ and $M_\star$.

M. C. Begelman & J. Dexter (2025) performed a more careful analysis of the transition to the radiative layer, which is more correctly termed the "inefficient convection (IE) layer" because energy transport by convection is still significant at this radius. Denoting the thickness of the outer layer as $\Delta r = R_\star - R_{\rm IE}$, they defined the boundary between efficient convection (which can be approximated with an adiabatic equation of state) and inefficient convection to be the point at which the radiative diffusion timescale $t_{\rm diff}$ across Δr becomes shorter than the buoyancy timescale $t_{\rm buoy}$. These timescales are defined as

$$t_{\rm diff} = \frac{\rho\kappa\Delta r^2}{c}, \qquad t_{\rm buoy} = R_\star\sqrt{\frac{\Delta r}{GM_\star}}. \tag{15}$$

Moreover, they found that about 8% of the quasi-star's mass lies in the IE layer. This means we can no longer assume the thin atmosphere approximation ($M_{\rm IE} = M_\star$), though for the purposes of finding the interior's boundary condition, the IE layer is likely not thick enough to necessitate modeling it.

In our models, we consistently saw that the radius at which $L = L_{\rm conv,max}$ (denoted R_c) lies below the base of the IE layer ($R_{\rm IE}$). Since it lies within the convective envelope, though, it can still be used as a stopping point for integrating the Lane-Emden equations, provided we can compute the mass here. We opt to use R_c as our stopping point rather than using $R_{\rm IE}$ (which would change the right hand side of Equation 14), as the real envelope will likely better resemble a 4/3 polytrope here than at the base of the IE layer.

To determine the mass M_c corresponding to this point, we have `MESA` find the mass coordinate at which $L = L_{\rm conv,max}$ in each time step. From the ratio $M_{\rm BH}/M_c$, we can then numerically find K_i. This uniquely determines $m_{\rm BH}$, so we can then compute $M_i = M_{\rm BH}/m_{\rm BH}$. One may wonder whether this would cause issues after the interior radius R_i exceeds R_c, since we would then not be able to use MESA to find a point in the envelope where $L = L_{\rm conv,max}$. Fortunately, this is not a problem, because R_c is in fact the theoretical limiting radius for R_i. This follows because R_c is, by definition, the maximum radius that could possibly support saturated convection (i.e. $L = L_{\rm conv,max}$); since the entire interior is assumed to be saturated, its boundary cannot exceed this point under the Coughlin model. As such, the Coughlin model has no theoretical solutions beyond $R_i = R_c$, corresponding to where $M_{\rm BH}/M_i = M_{\rm BH}/M_c \simeq 0.62$. This ratio does not depend on the scale of the quasi-star (such as its total mass or radius), and is thus said to be a "self-similar" property of the model across any scale.

For our implementation, we use a Mathematica notebook publicly released by Coughlin[1] to perform the numerical integrations for K_i and M_i, across a discrete set of mass ratios $M_{\rm BH}/M_\star$. We then perform a cubic spline interpolation on those points, allowing us to estimate these quantities at each time step.

We note that this model assumes the envelope can be approximated by a polytrope up to R_c, and Eq. 13 further assumes that the exponent of the polytrope is $\gamma_o = 4/3$. We considered using `MESA` to find the adiabatic index γ_o in the envelope at each time step, and then solving the more general Eq. 12 at the point where $L = L_{\rm conv,max}$. However, this would require either reintegrating Eq. 12 at every time step, or solving it across a grid of K_i and γ_o and doing a 2D interpolation. To save computational speed, we use the $\gamma_o = 4/3$ case at all times in the above expressions, allowing us to integrate Eq. 14 a priori with Mathematica. For use in future work exploring a dynamic adiabatic index, we generalized the equations of the Coughlin model to arbitrary γ_i and γ_o in this section; they reduce to those shown in E. R. Coughlin & M. C. Begelman (2024) upon setting $\gamma_i = \gamma_o = 4/3$.

Following E. R. Coughlin & M. C. Begelman (2024) and M. C. Begelman & J. Dexter (2025), we obtain R_i and M_c by assuming L approximately equals the Eddington luminosity of the quasi-star:

$$L_{\rm Edd} = \frac{4\pi G M_\star c}{\kappa}\,. \tag{16}$$

Here, κ is taken at the base of the inefficient convective layer (using the definition from M. C. Begelman & J. Dexter 2025). Similarly to before, we use MESA to determine the point in the star at which $t_{\rm diff} = t_{\rm buoy}$, and get the opacity there. With M_i and an approximation for L both known, R_i can then be computed via Eq. 9.

While we assume $L = L_{\rm Edd}$ to obtain the properties of the interior, the inner luminosity boundary condition is set to be $4\eta\pi R_i^2 p_i c_{s,i}$, where p_i and $c_{s,i}$ are obtained from the base of the envelope using MESA. This value is generally slightly higher than the computed Eddington luminosity, but results in several properties of the interior (e.g. p_i and $c_{s,i}$) being closer to their predicted values, compared to fixing the luminosity boundary condition to $L_{\rm Edd}$. Likewise, using $L_{\rm conv,max} = L_{\rm Edd}$ to find M_c is more stable and better matches predictions than using $L_{\rm conv,max} = L(r)$.

Other than the updated expressions for M_i, L and R_i, and implementation of the interpolation functions, the rest of our code remains structurally the same as with the Ball model. The relation $\dot{M}_{\rm BH} = L/\epsilon' c^2$ is still used to obtain the BH's growth rate, with ϵ' assumed to be approximately 0.1.

2.4. *Mass Loss Implementation*

We also explore the effects of including a mass loss scheme in our implementation of the Coughlin model. Eruptive winds in massive stars might originate from regions in the stellar envelopes where the local radiative luminosity exceeds the Eddington limit, causing radiative acceleration to overcome gravity and unbind material from the star (Y.-F. Jiang et al. 2018). These super-Eddington regions are usually associated with opacity peaks: in such layers, the increased opacity traps radiation, leading to density and gas-pressure inversions that

[1] https://github.com/erc-astro/mathematica/tree/main/quasi-stars

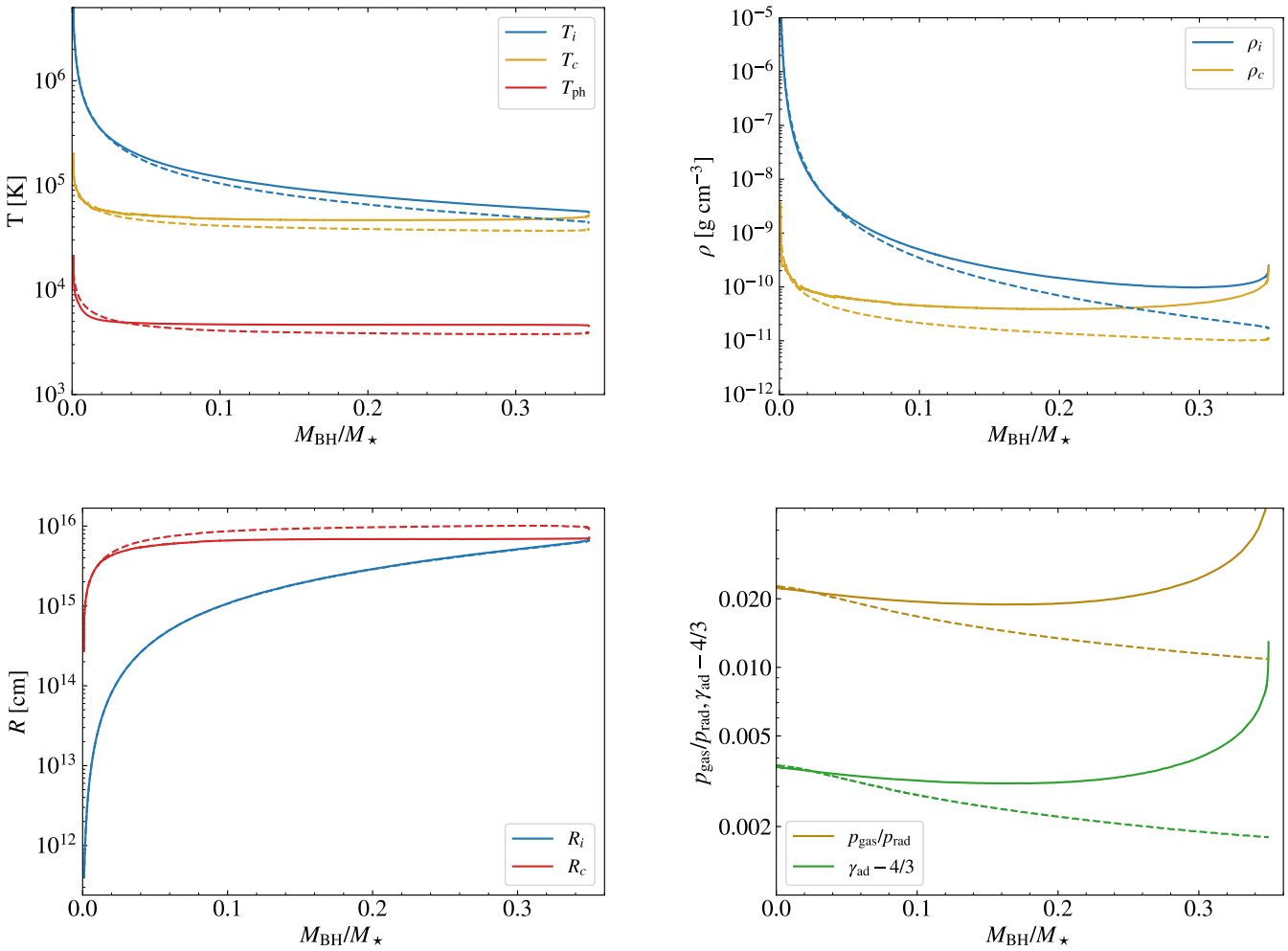

Figure 3. Comparison between various quasi-star properties (from top right, clockwise: density ρ, pressure ratio $p_{\rm gas}/p_{\rm rad}$ and adiabatic index $\gamma_{\rm ad}$, relevant radii R, temperature T) obtained with our `MESA` implementation of the baseline model of E. R. Coughlin & M. C. Begelman (2024) (solid lines) and the corresponding analytical predictions from the same work (dashed lines), shown over the course of the quasi-star's evolution. The total quasi-star mass is $M_\star = 10^5 M_\odot$. For a consistent comparison, the mass M_c in the analytical model (i.e. the mass at which $L = L_{\rm conv,max}$; see Eq. 13) is gradually adjusted to track the time-dependent value from the simulation.

destabilize the envelope (B. Paxton et al. 2013; Y.-F. Jiang et al. 2015; S. J. Cheng et al. 2024). When energy transport through convection becomes inefficient (below a critical optical depth $\tau < \tau_{\rm crit} \approx c/c_s$), excess radiative flux cannot be carried by convective motions and could instead drive episodic, dynamical mass ejections.[2] This mechanism effectively converts super-Eddington radiative luminosity into an outflow once the local radiative energy exceeds the binding energy of the overlying layers. This process is supported by 3D radiation-hydrodynamic simulations (e.g., Y.-F. Jiang et al. 2015, 2018) that show how turbulence and opacity peaks can lead to outbursts and sustained envelope oscillations. In the 1D framework implemented in `MESA` by S. J. Cheng et al. (2024), this is modeled by identifying layers where excess radiative energy exceeds gravitational binding energy, leading to eruptive mass loss.

In our implementation, we neglect the presence of other possible wind drivers and solely include this eruptive mass loss scheme using the `MESA` implementation developed by S. J. Cheng et al. (2024). A comparison of different wind prescriptions and their impact on

[2] We note, however, that this is one possible outcome. It has been pointed out that, if the mass across the outer layer is large, upwelling gas from the interior of the layer might not be propelled fast enough to escape. In this case, the radiation force imbalance might just create a turbulent but bound flow with large inhomogeneities where the radiation ultimately escapes through low-density channels with minor mass loss (e.g. C. Dotan & N. J. Shaviv 2012).

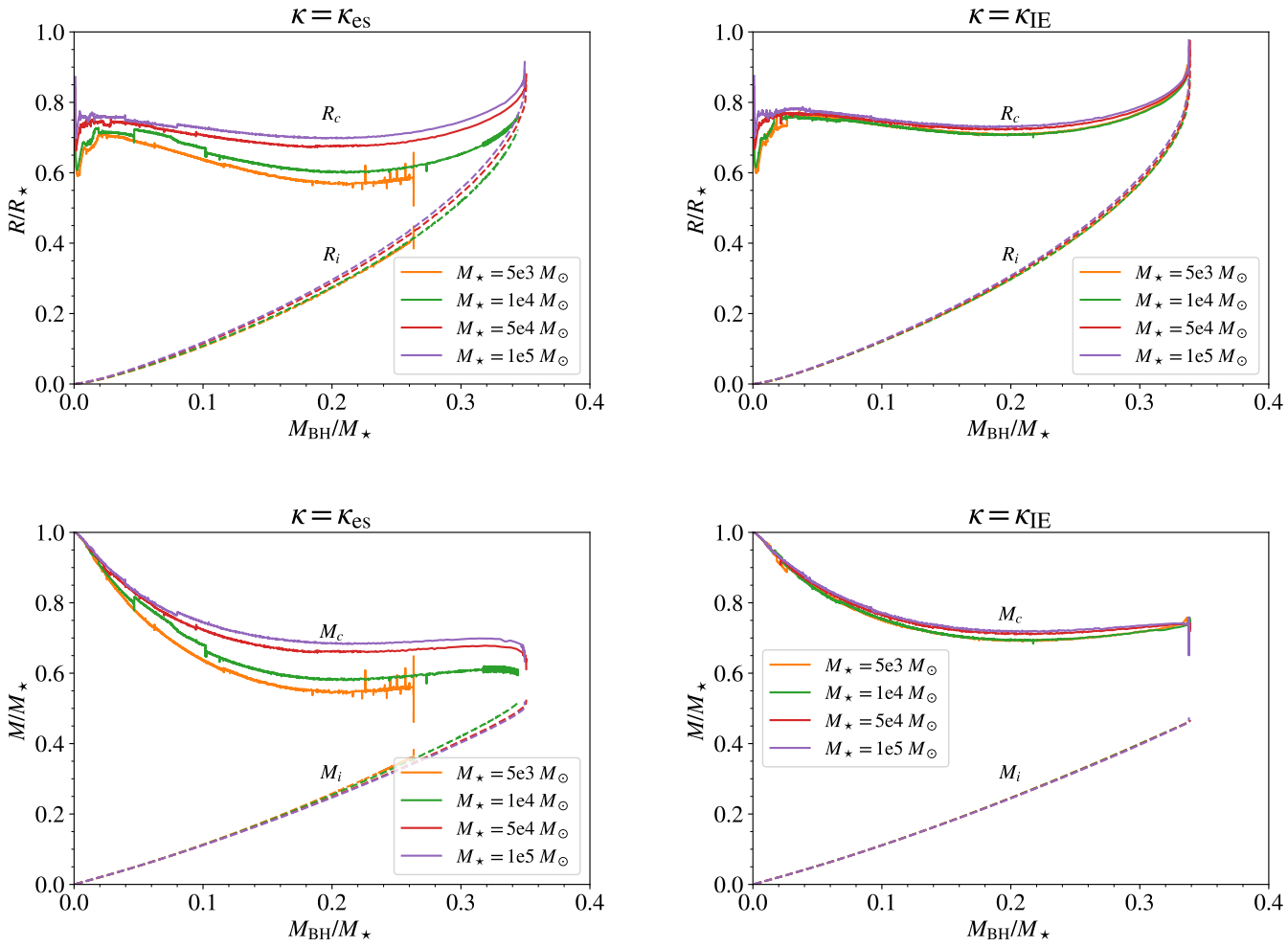

Figure 4. Comparison of R_c with R_i (top) and M_c with M_i (bottom), both when using $\kappa = \kappa_{\rm es} = 0.34\ {\rm cm}^2\ {\rm g}^{-1}$ (left) and using $\kappa = \kappa_{\rm IE}$ (right) for our calculation of $L_{\rm Edd}$, where $\kappa_{\rm IE}$ is the opacity taken at the base of the IE layer. All values shown here are normalized by the total radius or mass of the quasi-star. R_c and M_c are defined as the radius and mass at the point where $L_{\rm conv,max} = L_{\rm Edd}$.

quasi-star evolution is presented in A. D. Santarelli et al. (2025), whose study was conducted in parallel to ours and provides a complementary reference on this topic.

3. QUASI-STAR EVOLUTION AND BH GROWTH WITH MORE REALISTIC PRESCRIPTIONS

3.1. *Evolution with no mass loss*

As a first step, we create a model similar to that of E. R. Coughlin & M. C. Begelman (2024), and compare our numerical evolution with `MESA` with their semi-analytical predictions. We use a $M_\star = 10^5 M_\odot$ model and assume the electron scattering opacity $\kappa = \kappa_{\rm es} = 0.34\ {\rm cm}^2\ {\rm g}^{-1}$ in Eq. 16.

E. R. Coughlin & M. C. Begelman (2024) assume a thin atmosphere, such that M_c is practically the same as $M_\star$, and is thus kept fixed at $10^5\ M_\odot$ for this example. As described in M. C. Begelman & J. Dexter (2025), this approximation significantly overestimates the efficiency of convection in the star. Indeed, in our models M_c is time-dependent and generally well below $M_\star$. To account for this difference, and thus be able to compare our numerical results with their analytical ones, we modify their analytical predictions to use the same M_c for a given value of $M_{\rm BH}$ that we obtained from our model runs.

In Figure 3, we compare various properties of our $M_\star = 10^5\ M_\odot$ model with the analytical predictions from Figure 6 of E. R. Coughlin & M. C. Begelman (2024). As expected, our interior radii closely match the analytical predictions, since we are using the same equations for the interior as they do. On the other hand, the predicted values for R_c are approximately 1.2 times

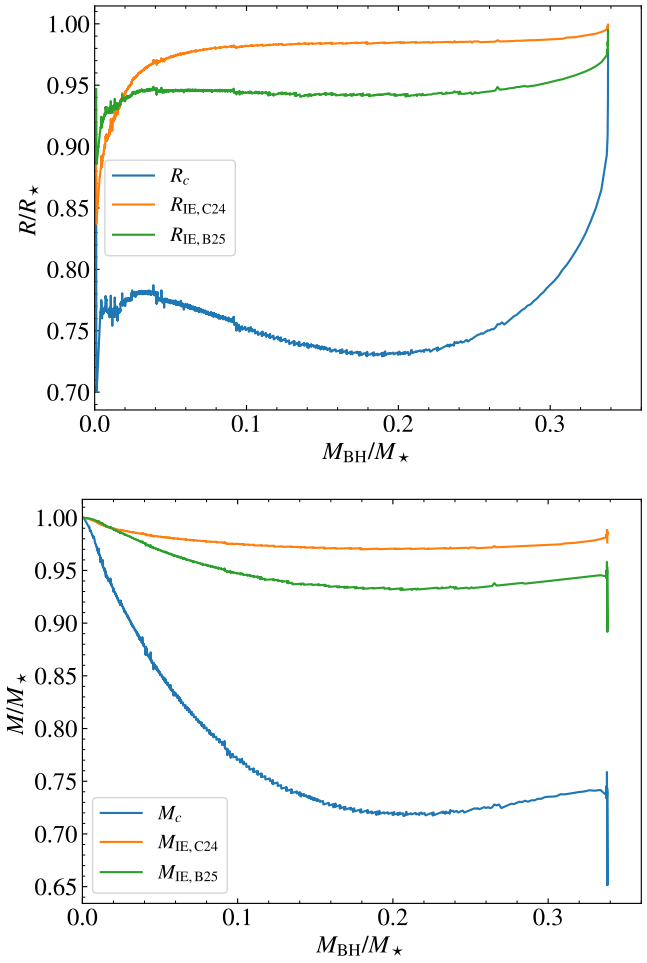

Figure 5. Top panel: Ratio of R_c and $R_{\rm IE}$ to the photospheric radius, as a function of the BH mass normalized to the quasi-star total mass. We show this radius using the definitions for the IE layer from both S. J. Cheng et al. (2024) (indicated with $M_{\rm IE,C24}$) and M. C. Begelman & J. Dexter (2025) (indicated with $M_{\rm IE,B25}$). The model here is a $M_\star = 10^5 M_\odot$ quasi-star with opacity taken from the base of the IE layer in the Eddington luminosity calculation. Bottom panel: Same as above, but showing the ratio of the masses below these points to the quasi-star's total mass.

larger than our results. Consequently, we reach $R_i \approx R_c$ more quickly, and our models therefore terminate at a lower ratio of $M_{\rm BH}/M_\star$ compared to the predictions in E. R. Coughlin & M. C. Begelman (2024) (although our final $M_{\rm BH}/M_i$ ratio of 0.66 is quite close to the predicted minimum of 0.62). Similarly, our other quasi-star properties at R_c (i.e. temperature, density, pressure) also differ somewhat from the analytical predictions.

The most noticeable of the deviations is the value for $p_{\rm gas}/p_{\rm rad}$ (and by extension, $\gamma_{\rm ad}$ as well) in the envelope, both of which are computed in the middle of the convective region. We see that our adiabatic index increases over time, as does the significance of gas pressure. Consequently, approximating the envelope with a $\gamma_o = 4/3$ polytrope would be less accurate at later times. We believe this to be the cause of the deviations between our results and Coughlin. In particular, the analytical prediction defines $R_c = \xi_c R_i$, where ξ_c is defined by Eq. 14. On the other hand, we identify R_c in our numerical modeling as the radius at which $L = L_{\rm conv,max}$. While the condition $L = L_{\rm conv,max}$ is equivalent to Eq. 14 for an ideal $\gamma_o = 4/3$ polytrope as described in Section 2.3 (for which the mass, pressure, and density are also continuous across the interior boundary), they are not identical in `MESA`, which models the convective region using a mixing-length theory. As expected, deviations become more pronounced as R_i approaches R_c and convection becomes less efficient.

Figure 3 also shows the quasi-star properties at the interior boundary. For our models, this is obtained from the base of the envelope using `MESA`. On the other hand, the analytical predictions for the properties at the interior boundary are derived using the equation of state for the interior region. While the two are generally of the same order of magnitude, the values we obtained from just above the boundary differ somewhat from the values they calculated from just below the boundary. As such, the temperature and pressure are not perfectly continuous across the interior boundary.

Having built a similar model to that of E. R. Coughlin & M. C. Begelman (2024), and compared our results with the semi-analytical predictions, we next focus on more realistic models. We now account for the envelope's mass decreasing as rest energy is converted to radiation; namely, we use Eq. 4 to obtain $\dot{M}_\star$, and use this to linearly approximate the mass at the following time step. We also allow κ to change over time in Eq. 16, by having `MESA` sample it at the base of the IE layer (which is defined by the condition $t_{\rm diff} = t_{\rm buoy}$; see Eq. 15). The conversion of mass to radiation generally results in the star losing $\sim 4\%$ of its mass by the end of the simulation, which has little effect on the results. On the other hand, the use of a dynamic opacity is more significant for less massive models, as they tend to have higher absorption opacities. In our $M_\star = 10^5\ M_\odot$ model, the opacity increases from ~ 0.35 to ~ 0.50 cm^2 g^{-1} over time; in contrast, the opacity in our $M_\star = 10^4\ M_\odot$ model reaches ~ 0.75 cm^2 g^{-1} by its end. Because the Eddington luminosity is inversely proportional to κ, this can slightly affect R_i and more noticeably affect M_c, as both are estimated using the Eddington luminosity.

In Figure 4, we compare the values of R_c and M_c with the radius and mass at the interior boundary, across several total quasi-star masses. We show our results when

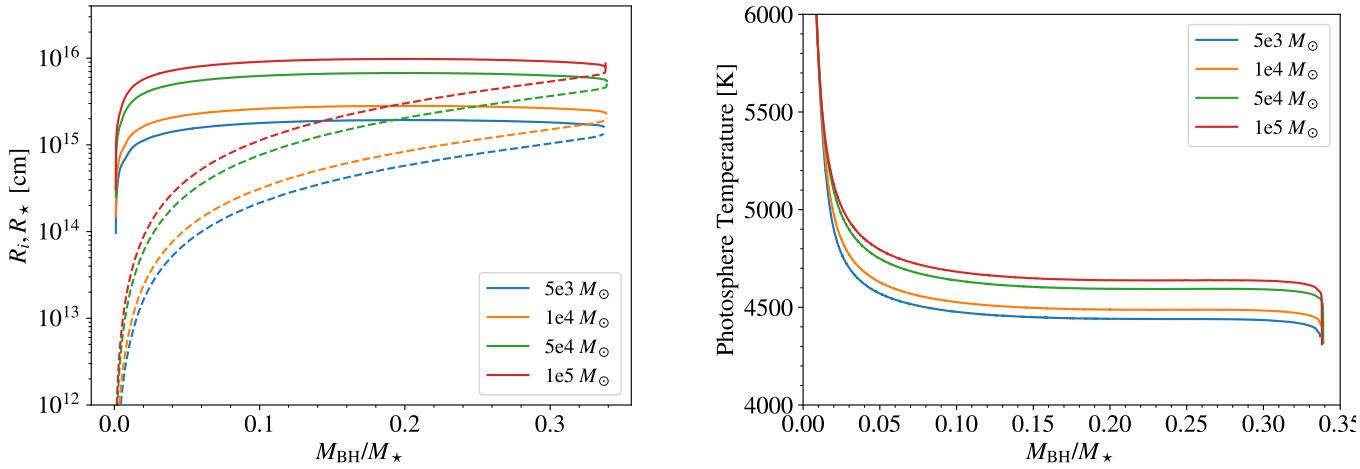

Figure 6. Left: The radii of the photosphere $R_\star$ (solid) and interior region R_i (dashed) for a range of quasi-star masses, with our `MESA` implementation of the Coughlin model. Right: photospheric temperatures for the same models. All models are initialized with the same properties, and an initial BH mass of $M_{\rm BH}/M_\star = 0.001$. The Eddington luminosity is calculated by taking κ at the base of the IE layer. It is apparent that the final ratio $M_{\rm BH}/M_\star$ is largely independent of the initial quasi-star mass.

approximating $\kappa = \kappa_{\rm es}$ in our calculation for $L_{\rm Edd}$, as well as taking κ at the base of the IE layer using `MESA`. When taking $\kappa = \kappa_{\rm es}$, we very clearly see that the region below R_c is larger relative to the quasi-star in more massive models, a similar phenomenon to what occurs in sufficiently large normal stars. However, this effect is much less pronounced if we take κ at the base of the IE layer; indeed, this increases $L_{\rm Edd}$ to a greater degree for less massive quasi-stars, and consequently increases the mass and radius below $L_{\rm conv,max} = L_{\rm Edd}$. In practice, this allows less massive quasi-stars to evolve to nearly the same $M_{\rm BH}/M_\star$ ratio as more massive stars.

We also see that M_c does not quite match M_i at the end of the runs. This is likely because M_c is approximated here by using $L_{\rm Edd}$; while this gave us much more stable results than using $L = 4\pi\eta R_i^2 \rho_i c_{s,i}$, it does overestimate the maximum possible radius that M_i can reach. In all of our models, $M_{\rm BH}/M_i$ falls within the range $0.66 - 0.72$ at the end of the run, which is still reasonably close to the theoretical limit of 0.62.

Because less massive quasi-stars are expected to have higher opacities, we will focus on the dynamic κ models from here on, as we consider it the more physically motivated model.

Figure 5 shows how the mass and radius of the system below the IE layer, $M_{\rm IE}$, changes over time. For the definition from M. C. Begelman & J. Dexter (2025) (green line marked with B25), we find $M_{\rm IE}/M_\star \sim 0.93$ for most of the evolution, consistent with their estimate of the IE layer containing $\sim 8\%$ of the quasi-star's total mass. As expected, R_c (the point at which the energy transfer cannot be entirely convective) lies below the definitions of the IE layer from both M. C. Begelman & J. Dexter (2025) and S. J. Cheng et al. (2024), which are based on whether convective energy transfer is inefficient compared to radiative transfer. This justifies our use of Eq. 14, as it requires M_c to lie within the convectively-efficient region. It should be noted in these plots that $R_\star$ changes over time, whereas $M_\star$ does not; for example, the photospheric radius decreases near the end of the run, while R_c remains more or less static. This causes $R_c/R_\star$, and not $M_c/M_\star$, to rise to unity.

In Figure 6, we compare the photospheric radii and temperature for models with various masses, as a function of $M_{\rm BH}/M_\star$. These models all use a dynamic κ; as we showed in Figure 4, $M_c/M_\star$ is approximately constant across the evolution in this scenario. Since the maximum $M_{\rm BH}/M_c$ is a self-similar property of the model, this results in all of these models terminating at approximately the same $M_{\rm BH}/M_\star$ ratio.

In Figure 7, we show density and pressure profiles for our $M_\star = 10^5 M_\odot$ model. While the density profile is virtually monotonically decreasing for very small BH masses ($M_{\rm BH}/M_\star \sim 10^{-3}$), density inversions begin to manifest near the surface for $M_{\rm BH}/M_\star \sim 10^{-2}$ onwards. As described in M. C. Begelman & J. Dexter (2025) and S. J. Cheng et al. (2024), the existence of these inversions is expected near the transition to the IE layer: convection becomes inefficient near the surface, and the radiative flux slightly exceeds the local Eddington value. The resulting imbalance leads to a region where the outward radiation force drives material upward, and hydrostatic equilibrium can only be maintained if the gas pressure increases outward, implying

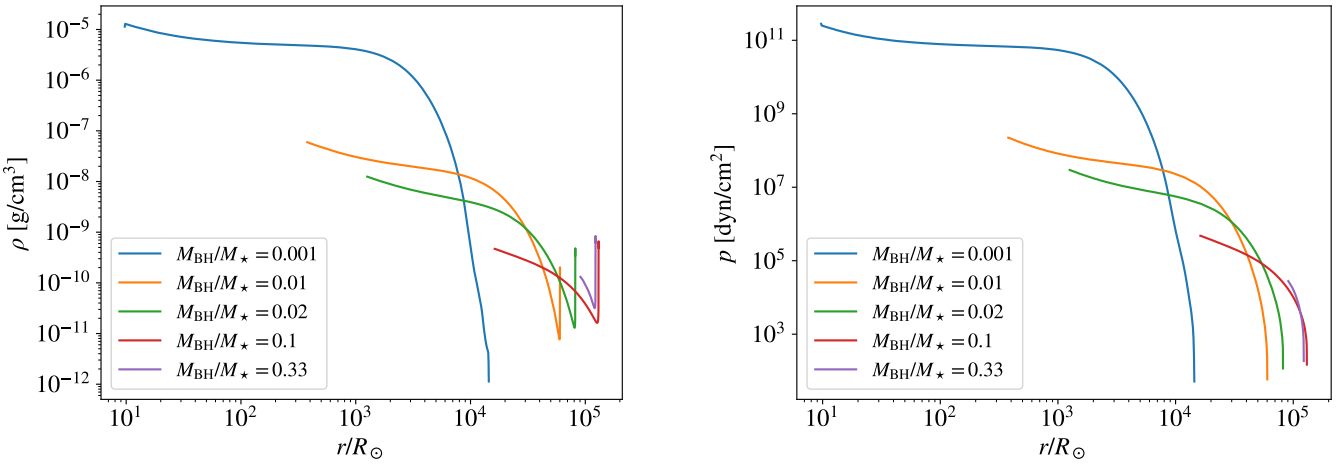

Figure 7. Density (left) and total pressure (right) profiles for the $M_\star = 10^5 M_\odot$ Coughlin model at several values of $M_{\rm BH}/M_\star$ during the quasi-star evolution. Only the density at radii $r > R_i$ is plotted. Note the density inversion which starts to appear during the later phases of evolution when convection becomes inefficient near the surface.

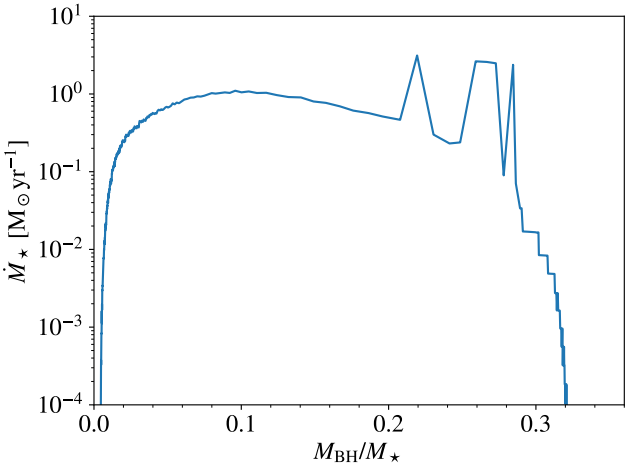

Figure 8. Wind mass loss rate during the quasi-star evolution, for a Coughlin model with initial mass $M_\star = 10^5 M_\odot$ and mass loss due to eruptive winds.

a density inversion (a rise in density with radius). On the other hand, the profile for the total pressure does not display such an inversion, as a result of the fact that `MESA` strives to maintain hydrostatic equilibrium.

3.2. *Evolution with mass loss*

For our $M_\star = 10^5\ M_\odot$ Coughlin model, we also implemented the wind scheme from S. J. Cheng et al. (2024) described in Section 2.4. We take the wind efficiency factor to be 0.1 (see Eq. 12 of S. J. Cheng et al. 2024).

The predicted mass loss rate as a function of $M_{\rm BH}/M_\star$ during the quasi-star evolution is shown in Figure 8. Winds manifest early on, and cease at approximately $M_{\rm BH}/M_\star \sim 0.31$. We find that these winds greatly reduce the quasi-star's mass over time, leaving it with a total mass of $\sim 4.5 \times 10^3 M_\odot$ by the end of the run (less than 1/20 of its original mass).

Figure 9 compares the Eddington factor $\Gamma = L/L_{\rm Edd}$ throughout the quasi-star with the temperature profile, both during the onset, peak, and end of the wind mass loss. The start of mass loss corresponds to the formation of a spike in opacity, causing $\Gamma_{\rm Edd,rad}$ to rise in the IE layer. As the quasi-star evolves, the IE layer becomes increasingly dense, causing the optical depths in this region to rise. $\tau_{\rm crit}$ also increases, albeit at a slower rate than the optical depths near the surface of the quasi-star; this causes the region for which $\tau < \tau_{\rm crit}$ (in other words, the IE layer) to shrink. Eventually, the IE layer becomes so thin that $\Gamma_{\rm Edd,rad} < 1$ everywhere in it, causing the winds to cease. At this point, we still have $\Gamma_{\rm Edd,rad} > 1$ slightly below the IE layer, but super-Eddington luminosities below the IE layer are not assumed to contribute to winds in this model.

Figure 10 shows the evolution of the quasi-star's luminosity versus its photospheric temperature (effectively an "HR diagram") for the same $M_\star = 10^5\ M_\odot$ model, with and without winds. Once the BH is injected, the star gradually expands and progresses rightward toward cooler effective temperatures, with its luminosity approximately at the Eddington limit. At an age of $t \approx 1.5 \times 10^5$ yr, the opacity sharply spikes up near the surface of the quasi-star and a density inversion forms. In the model without winds, we see this correspond to an increase in luminosity past the Eddington limit. Near the end of the quasi-star's lifetime, the luminosity then begins to drop, corresponding to a drop in temperature (cfr. Figure 6, right panel). With the implementation of stellar winds, on the other hand, the opacity spike

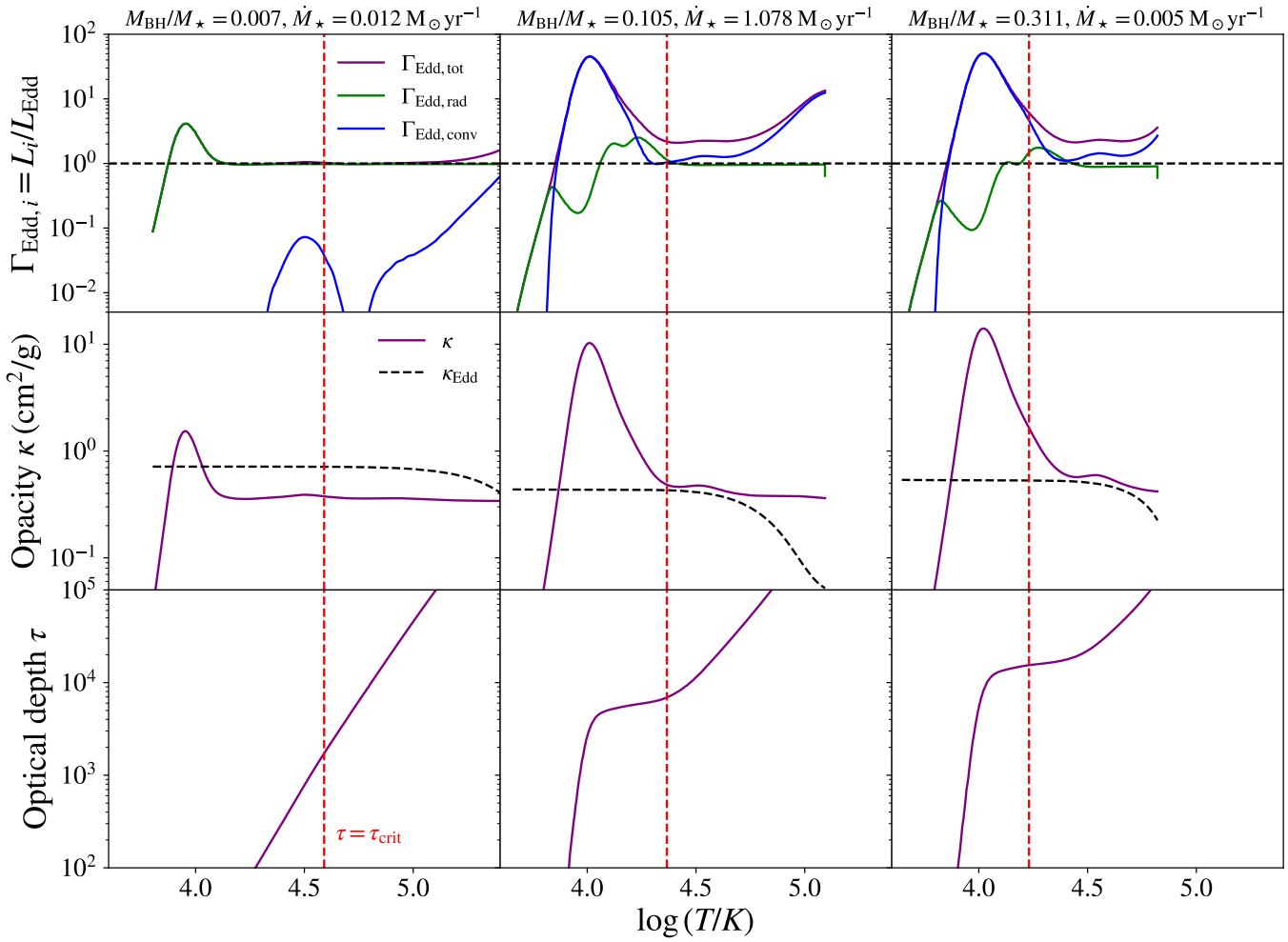

Figure 9. Profiles of luminosity in Eddington units (top row), opacity (middle row), and optical depth (bottom row) for our 10^5 $M_\odot$ quasi-star model with eruptive winds enabled. Left column: Snapshot taken during the start of wind mass loss ($M_{BH}/M_\star = 0.007$); Middle column: Snapshot taken during the presence of strong winds ($M_{BH}/M_\star = 0.105$); Right column: Snapshot when winds have almost entirely ceased ($M_{BH}/M_\star = 0.311$). The vertical red dashed line shows the location of the convectively-inefficient layer ($\tau < \tau_{crit}$). Eruptive mass loss only occurs if $\Gamma_{Edd,rad}$ exceeds 1 in this part of the model, and ceases entirely when $\Gamma_{Edd,rad} \leq 1$ to the left of the red line .

triggers eruptive mass loss. As the mass $M_\star$ drops, so does the Eddington limit and therefore the luminosity.

Figure 11 shows the evolution of R_c and R_i for the same $M_{\star,init} = 10^5 M_\odot$ model, with winds (solid) and without winds (dashed). Winds begin to cause significant deviations from the fixed $M_\star$ model starting around $M_{BH}/M_\star \sim 0.01$. Near the end of the evolution, at around $M_{BH}/M_\star \sim 0.31$, mass loss quickly drops, causing both R_i and R_c to suddenly start evolving as they would for a fixed (albeit now much smaller) $M_\star$. It is important to point out that, although $M_{BH}/M_\star$ is used as the horizontal axis, $M_\star$ is virtually constant for the non-wind model but is changing for the wind model. Thus, the wind model actually has a significantly shorter lifespan than the non-wind model (2.1 Myr for the wind model, compared to 16.6 Myr for the non-wind model).

As noted earlier, certain aspects of the Coughlin solution are self-similar, meaning they are consistent across different physical scales (e.g. for different values of $M_\star$). For example, the final value of M_{BH}/M_i is largely independent of the value of $M_\star$. Since κ increases over time at the base of the IE layer, this model also ends at a very similar (albeit slightly smaller) value of M_{BH}/M_c to the non-winds model (cf. Fig 4).

Figure 12 shows Kippenhahn diagrams for the $10^5 M_\odot$ quasi-star model, both with and without winds. These diagrams display how different regions inside a star evolve as the star ages. Prior to the onset of mass loss, the BH and the saturated convection region gradually grow over time. In the non-wind model, we see that the BH initially comprises almost all of the interior's mass,

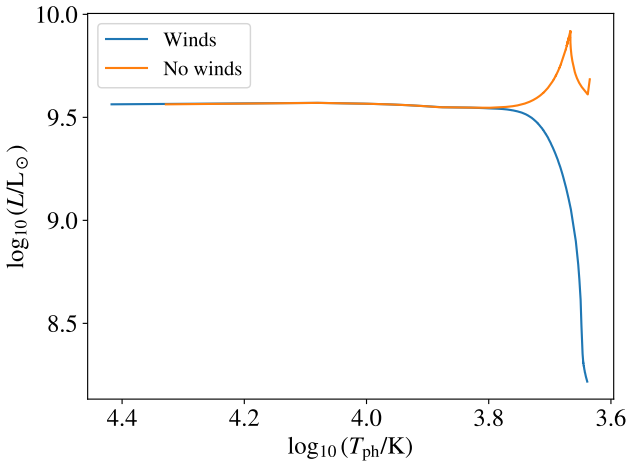

Figure 10. Hertzsprung–Russell diagram of a quasi-star of initial mass $10^5\ M_\odot$, evolving according the the Coughlin model, and considering both models with and without mass loss.

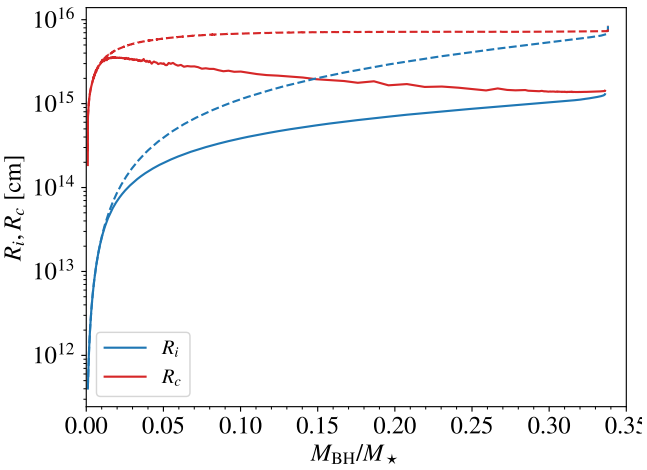

Figure 11. Values of R_c and R_i for the Coughlin model with winds (solid lines) and without winds (dashed lines), as a function of the ratio of the BH mass to the quasi-star mass. The initial quasi-star mass is $M_\star = 10^5 M_\odot$. In the case with winds, this decreases with time.

and gas becomes an increasingly significant portion of it over time.

Once mass loss begins, $M_\star$ decreases rapidly, causing a concomitant reduction in the Eddington luminosity of the quasi-star (cf. Eq. 16). The growth rate of the BH likewise drops, as it is proportional to the luminosity (Eq. 4). While the mass of the BH remains nearly constant during this brief period, the mass of the quasi-star (and consequently, M_c as well) greatly decreases, and the ratio $M_{\rm BH}/M_c$ therefore increases. In other words, our model quickly shifts from being a large quasi-star with a relatively small BH, to being a smaller quasi-star with a relatively large BH. After the winds finally cease, the BH continues evolving as it would for a $M_\star = 4.5 \times 10^3 M_\odot$ quasi-star late in its life.

4. SUMMARY AND FUTURE DIRECTIONS

The discovery of extremely massive BHs at very high redshifts has posed a long-standing problem regarding how such objects could have formed within a short time after the beginning of the universe. This issue has become more pressing in recent years with the JWST discovery of the LRDs, for which rapidly accreting BHs represent a compelling interpretation. Among the proposed scenarios of early BH growth, quasi-stars (M. C. Begelman et al. 2008; M. C. Begelman & J. Dexter 2025) constitute a prominent candidate.

In this work, we have presented a numerical investigation of quasi-stars through dedicated modifications to the public stellar evolution code `MESA`. We examined the growth of the central BH under various assumptions for the inner boundary condition, determined by the physical properties of the region surrounding the accreting BH. In addition, we investigated the influence of the outer convectively-inefficient layer and the potential impact of mass loss through winds.

Our investigation proceeded through increasing levels of complexity, and our main findings are summarized as follows:

- We began by implementing the quasi-star models by W. H. Ball et al. (2011, 2012), characterized by an inner boundary condition set at a multiple N of the Bondi radius. For a fixed total quasi-star mass, our numerical simulations for the W. H. Ball et al. (2012) model consistently terminated when the black hole mass reached a critical value that depends on N, given by $M_{\rm crit}(N) = c_{s,i}^3/(12\sqrt{N^3 G^3 \pi \rho_i})$, which is a limit we independently derived analytically. Although the dependence of the maximum mass on N has previously been noted and derived by E. R. Coughlin & M. C. Begelman (2024), our analytical expression provides a closer match to the numerical results, particularly for smaller values of N.

- We next implemented in `MESA` a quasi-star model developed by E. R. Coughlin & M. C. Begelman (2024), in which an inner convective region is matched to an outer adiabatic envelope. We found that the BH grows to a fraction $\approx 33\%$ of the quasi-star mass, roughly independent of the initial mass of the quasi-star. We demonstrated that the factor of ~ 2 discrepancy between our maximum

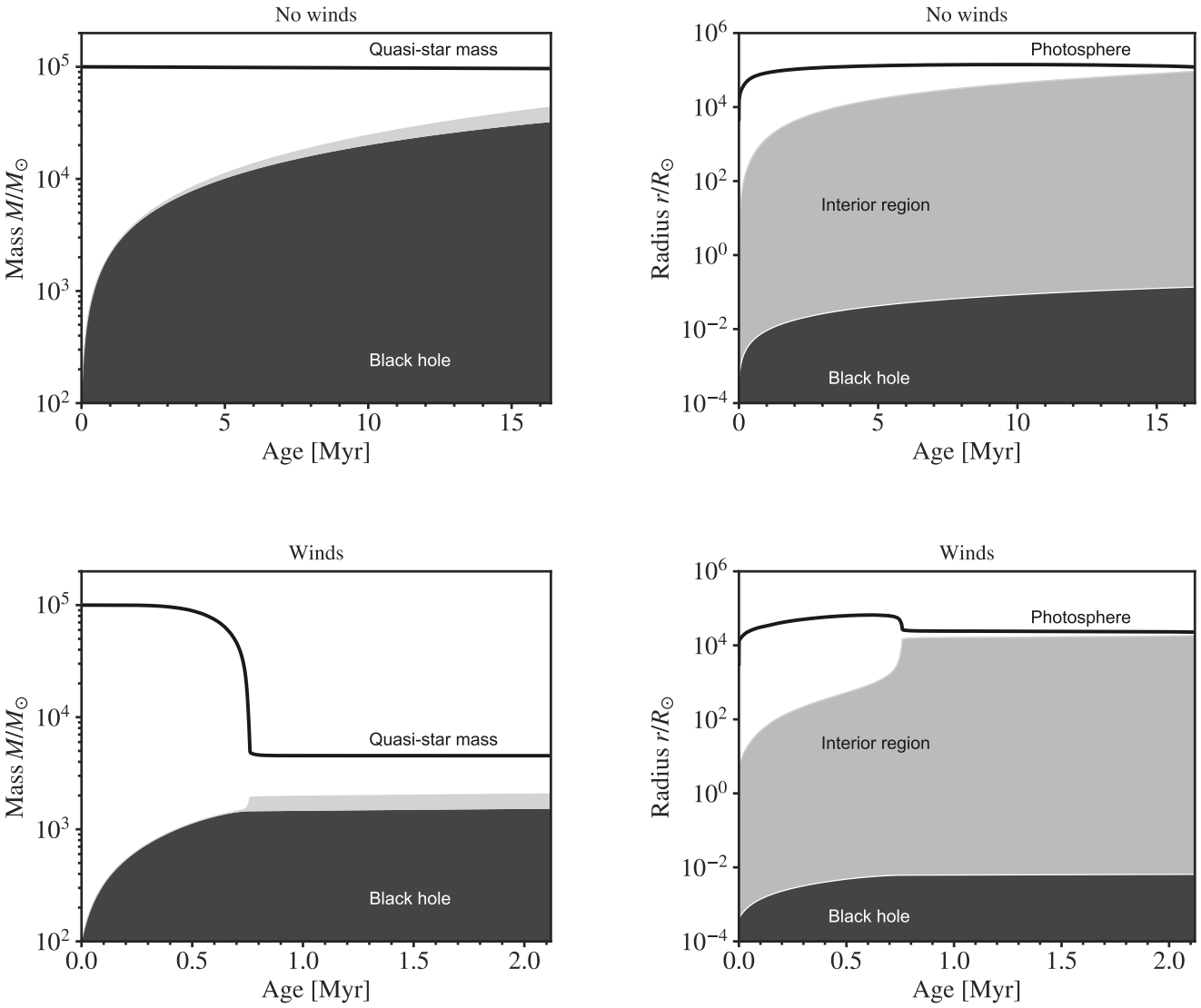

Figure 12. Kippenhahn diagrams for the $M_\star = 10^5\ M_\odot$ model, both without winds (top) and with winds (bottom). Dark gray regions correspond to the BH; light gray corresponds to the saturated convection region, and white corresponds to the envelope.

BH mass and that derived by E. R. Coughlin & M. C. Begelman (2024) arises from their assumption that M_c, the maximum mass at which convection could account for all the energy transfer in the envelope, remains equal to $M_\star$ throughout the quasi-star evolution. In other words, they assume M_i can grow up to $M_\star$, so that their predicted limit of $M_{\rm BH}/M_i \sim 0.62$ is equivalent to $M_{\rm BH}/M_\star \sim 0.62$. We do not make this assumption, so while our final $M_{\rm BH}/M_i$ is close to the prediction, our final $M_{\rm BH}/M_\star$ differs from it.

We also sought to better estimate the star's luminosity in the Coughlin model, which is approximated by the Eddington limit. Instead of assuming $\kappa = \kappa_{\rm es} = 0.34\ {\rm cm}^2\ {\rm g}^{-1}$, we have `MESA` find the opacity at the base of the IE layer. When making this adjustment, our models terminated at roughly $M_{\rm BH}/M_\star \sim 0.33$ across all our choices of $M_\star$.

The photospheric temperatures of quasi-stars are found to decrease over time and, except during the very early stages of their evolution, lie in the range $\sim 4500 - 4800$ K for the range of quasi-star masses we studied, with higher masses naturally corresponding to higher effective temperatures.

- We next implemented eruptive winds into our `MESA` version of the Coughlin quasi-star model, following the prescription of S. J. Cheng et al. (2024),

and examined their impact for a fiducial case with $M_\star = 10^5 M_\odot$. We find that the inclusion of winds not only shortens the quasi-star's lifetime but can also lead to substantial mass depletion. In the case studied, the final stellar mass was reduced to approximately one-twentieth of its initial value. Notably, the final BH–to–quasi-star mass ratio remains roughly the same as in the wind-free case, as do other self-similar properties of the Coughlin model.

Our investigation represents an additional step toward understanding black hole growth within quasi-stars, and thereby their potential role as progenitors of supermassive BHs in the early universe, as well as possible sources of LRDs, should these indeed correspond to accreting BHs as suggested by some observational evidence.

We anticipate several directions for future work. First, since quasi-stars are expected to form in very dense environments, accretion onto them is likely to play a significant role. In fact, the presence of accretion during the quasi-star's lifetime appears to be essential for substantial BH growth, given the potentially disruptive effect of winds, which can greatly reduce the quasi-star's mass and, consequently, the mass of the BH forming within it.

Another important step toward connecting quasi-stars to their observable properties, and thus more quantitatively assessing the suggestion by M. C. Begelman & J. Dexter (2025) that they may be progenitors of LRDs, will be a more detailed treatment of their outer layers, and particularly the opacity, with the aim of predicting the spectral energy distributions of quasi-stars.

The overall stability of quasi-stars presents another intriguing avenue for investigation. Hyper-accretion onto BHs is known to drive powerful outflows and jets. If the infalling gas possesses angular momentum, an accretion disk may form around the central BH, creating conditions conducive to jet formation. Whether a quasi-star can remain stable over an extended period under such circumstances—and, if so, what its resulting observational signatures might be—remains an open question for future study.

ACKNOWLEDGMENTS

JBH and RP acknowledge support from NASA award 80NSSC25K7554. JBH and PJA acknowledge support from award 644616 from the Simons Foundation. MCB acknowledges support from NASA Astrophysics Theory Program grants 80NSSC22K0826 and 80NSSC24K0940. The Center for Computational Astrophysics at the Flatiron Institute is supported by the Simons Foundation.

REFERENCES

Akins, H. B., Casey, C. M., Lambrides, E., et al. 2025, ApJ, 991, 37, doi: 10.3847/1538-4357/ade984

Bañados, E., Venemans, B. P., Mazzucchelli, C., et al. 2018, Nat., 553, 473, doi: 10.1038/nature25180

Ball, W. H., Tout, C. A., & Żytkow, A. N. 2012, M.N.R.A.S., 421, 2713, doi: 10.1111/j.1365-2966.2012.20508.x

Ball, W. H., Tout, C. A., Żytkow, A. N., & Eldridge, J. J. 2011, M.N.R.A.S., 414, 2751, doi: 10.1111/j.1365-2966.2011.18591.x

Barro, G., Perez-Gonzalez, P. G., Kocevski, D. D., et al. 2024, arXiv e-prints, arXiv:2412.01887, doi: 10.48550/arXiv.2412.01887

Begelman, M. C., & Dexter, J. 2025, arXiv e-prints, arXiv:2507.09085, doi: 10.48550/arXiv.2507.09085

Begelman, M. C., Rossi, E. M., & Armitage, P. J. 2008, M.N.R.A.S., 387, 1649, doi: 10.1111/j.1365-2966.2008.13344.x

Begelman, M. C., Volonteri, M., & Rees, M. J. 2006, M.N.R.A.S., 370, 289, doi: 10.1111/j.1365-2966.2006.10467.x

Bellinger, E. P., Caplan, M. E., Ryu, T., et al. 2023, ApJ, 959, 113, doi: 10.3847/1538-4357/ad04de

Bondi, H. 1952, M.N.R.A.S., 112, 195, doi: 10.1093/mnras/112.2.195

Campbell, C. B., Santarelli, A. D., & Caplan, M. E. 2025, Research Notes of the American Astronomical Society, 9, 185, doi: 10.3847/2515-5172/adef33

Cheng, S. J., Goldberg, J. A., Cantiello, M., et al. 2024, The Astrophysical Journal, 974, 270, doi: 10.3847/1538-4357/ad701e

Coughlin, E. R., & Begelman, M. C. 2024, ApJ, 970, 158, doi: 10.3847/1538-4357/ad5723

Dotan, C., Rossi, E. M., & Shaviv, N. J. 2011, M.N.R.A.S., 417, 3035, doi: 10.1111/j.1365-2966.2011.19461.x

Dotan, C., & Shaviv, N. J. 2012, M.N.R.A.S., 427, 3071, doi: 10.1111/j.1365-2966.2012.22020.x

Fan, X., Strauss, M. A., Becker, R. H., et al. 2006, AJ, 132, 117, doi: 10.1086/504836

Fiacconi, D., & Rossi, E. M. 2017, M.N.R.A.S., 464, 2259, doi: 10.1093/mnras/stw2505

Furtak, L. J., Zitrin, A., Plat, A., et al. 2023, ApJ, 952, 142, doi: 10.3847/1538-4357/acdc9d

Greene, J. E., Labbe, I., Goulding, A. D., et al. 2024, ApJ, 964, 39, doi: 10.3847/1538-4357/ad1e5f

Jiang, Y.-F., Cantiello, M., Bildsten, L., Quataert, E., & Blaes, O. 2015, ApJ, 813, 74, doi: 10.1088/0004-637X/813/1/74

Jiang, Y.-F., Cantiello, M., Bildsten, L., et al. 2018, Nat., 561, 498, doi: 10.1038/s41586-018-0525-0

Kocevski, D. D., Finkelstein, S. L., Barro, G., et al. 2025, ApJ, 986, 126, doi: 10.3847/1538-4357/adbc7d

Kokorev, V., Caputi, K. I., Greene, J. E., et al. 2024, ApJ, 968, 38, doi: 10.3847/1538-4357/ad4265

Labbé, I., van Dokkum, P., Nelson, E., et al. 2023, Nat., 616, 266, doi: 10.1038/s41586-023-05786-2

Liu, H., Jiang, Y.-F., Quataert, E., Greene, J. E., & Ma, Y. 2025, arXiv e-prints, arXiv:2507.07190, doi: 10.48550/arXiv.2507.07190

Matthee, J., Naidu, R. P., Brammer, G., et al. 2024, ApJ, 963, 129, doi: 10.3847/1538-4357/ad2345

Paxton, B., Bildsten, L., Dotter, A., et al. 2011, The Astrophysical Journal Supplement Series, 192, 3, doi: 10.1088/0067-0049/192/1/3

Paxton, B., Cantiello, M., Arras, P., et al. 2013, The Astrophysical Journal Supplement Series, 208, 4, doi: 10.1088/0067-0049/208/1/4

Paxton, B., Marchant, P., Schwab, J., et al. 2015, The Astrophysical Journal Supplement Series, 220, 15, doi: 10.1088/0067-0049/220/1/15

Paxton, B., Schwab, J., Bauer, E. B., et al. 2018, The Astrophysical Journal Supplement Series, 234, 34, doi: 10.3847/1538-4365/aaa5a8

Paxton, B., Smolec, R., Schwab, J., et al. 2019, The Astrophysical Journal Supplement Series, 243, 10, doi: 10.3847/1538-4365/ab2241

Santarelli, A. D., Campbell, C. B., Farag, E., et al. 2025, arXiv e-prints, arXiv:2510.11772, doi: 10.48550/arXiv.2510.11772

Setton, D. J., Greene, J. E., de Graaff, A., et al. 2024, arXiv e-prints, arXiv:2411.03424, doi: 10.48550/arXiv.2411.03424

Taylor, A. J., Finkelstein, S. L., Kocevski, D. D., et al. 2025, ApJ, 986, 165, doi: 10.3847/1538-4357/add15b

Volonteri, M., & Begelman, M. C. 2010, M.N.R.A.S., 409, 1022, doi: 10.1111/j.1365-2966.2010.17359.x

APPENDIX

A. DERIVATION OF CORRECTED BONDI RADIUS

In W. H. Ball et al. (2012), the Bondi radius is given by

$$R_i = N\frac{2G(M_{\rm BH}+M_{\rm cav})}{c_{s,i}^2} = N\frac{2G}{c_{s,i}^2}\left(M_{\rm BH}+\frac{8\pi\rho_i}{3}R_i^3\right)$$

$$R_i^3 - \frac{3c_{s,i}^2}{16\pi NG\rho_i}R_i + \frac{3M_{\rm BH}}{8\pi\rho_i} = 0$$

The discriminant of this depressed cubic is

$$\Delta = \frac{243}{64\pi^2\rho_i^2}\left(M_{\rm crit}^2 - M_{\rm BH}^2\right)$$

where we define $M_{\rm crit} = c_{s,i}^3/12\sqrt{N^3G^3\pi\rho_i}$.

Consider the case $M_{\rm BH} > M_{\rm crit}$. Then $\Delta < 0$, so by Cardano's formula,

$$R_i = \left(-A-\sqrt{A^2-B^3}\right)^{1/3} + \left(-A+\sqrt{A^2-B^3}\right)^{1/3}$$

where we denote

$$A = \frac{3M_{\rm BH}}{16\pi\rho_i} \quad B = \frac{c_{s,i}^2}{16\pi\rho_i NG}.$$

Since R_i must be positive, it follows that

$$\left(-A-\sqrt{A^2-B^3}\right)^{1/3} > -\left(-A+\sqrt{A^2-B^3}\right)^{1/3}$$

$$-A-\sqrt{A^2-B^3} > A-\sqrt{A^2-B^3}$$

$$-A > A$$

This means A must be negative, which is unphysical (since A is defined in terms of positive quantities). Thus, there is no valid solution for $M_{\rm BH} > M_{\rm crit}$.

Now consider the case $M_{\rm BH} = M_{\rm crit}$. Then $\Delta = 0$, so the roots of the cubic are

$$R_i = \frac{3NGM_{\rm crit}}{c_{s,i}^2}, \quad -\frac{6NGM_{\rm crit}}{c_{s,i}^2}.$$

Obviously, only the positive solution can be physical.

Finally, consider the case $M_{\rm BH} < M_{\rm crit}$. Then $\Delta > 0$, so there are three distinct trigonometric solutions. For $k = 0, 1, 2$, we have

$$R_i = \frac{6NGM_{\rm crit}}{c_{s,i}^2}\cos\left(\frac{\arccos(-M_{\rm BH}/M_{\rm crit}) - 2\pi k}{3}\right)$$

$$= \frac{6NGM_{\rm crit}}{c_{s,i}^2}\cos\left(\frac{\arccos(M_{\rm BH}/M_{\rm crit}) + \pi(2k-1)}{3}\right).$$

The only choice satisfying the boundary condition $R_i(M_{\rm BH}\to 0) = 0$ is $k = 1$. Thus, this is the only physically valid trigonometric solution:

$$R_i = \frac{6NGM_{\rm crit}}{c_{s,i}^2}\cos\left(\frac{\arccos(M_{\rm BH}/M_{\rm crit}) + \pi}{3}\right).$$

If we set $M_{\rm BH} = M_{\rm crit}$ in this formula, we recover $R_i = 3NGM_{\rm crit}/c_{s,i}^2$. Hence, the Bondi radius is given by this formula for $M_{\rm BH} \le M_{\rm crit}$, and there are no physical solutions for $M_{\rm BH} > M_{\rm crit}$.